

The Brieva-Rook Localization of the Microscopic Nucleon-Nucleus Potential

Kosho Minomo,^{1,*} Kazuyuki Ogata,^{1,†} Michio Kohno,^{2,‡}

Yoshifumi R. Shimizu,^{1,§} and Masanobu Yahiro^{1,¶}

¹*Department of Physics, Kyushu University, Fukuoka 812-8581, Japan*

²*Physics Division, Kyushu Dental College, Kitakyushu 803-8580, Japan*

(Dated: November 3, 2018)

Abstract

The nonlocality of the microscopic nucleon-nucleus optical potential is commonly localized by the Brieva-Rook approximation. The validity of the localization is tested for the proton+⁹⁰Zr scattering at the incident energies from 65 MeV to 800 MeV. The localization is valid in the wide incident-energy range.

PACS numbers:

*minomo@phys.kyushu-u.ac.jp

†ogata@phys.kyushu-u.ac.jp

‡kohno@kyu-dent.ac.jp

§shimizu@phys.kyushu-u.ac.jp

¶yahiro@phys.kyushu-u.ac.jp

I. INTRODUCTION

Microscopic understanding of nucleon-nucleus (NA) elastic scattering is a long-standing fundamental subject in the nuclear reaction theory. This is nothing but to solve the many-body scattering problem. The many-body collision, however, can be approximately described as a scattering between two bodies interacting via a complex mean-field (optical) potential. This optical potential is an important ingredient in theoretical calculations of cross sections of elastic and inelastic scattering, charge exchange and transfer reactions, and so on. This means that a good global optical model is a powerful tool for predicting observables of NA scattering for which no measurements exist, e.g., scattering of unstable nuclei from proton target.

A reasonable way of getting the optical potential is to calculate the NA folding potential with the nucleon-nucleon (NN) g -matrix interaction [1, 2, 3, 4, 5, 6]. The interaction is first evaluated in infinite nuclear matter and then folded into target (A) density by using the local-density approximation. The g -matrix interaction thus obtained is a complex nonlocal potential depending on the incident energy (E) of nucleon (N) and the nuclear-matter density (ρ). This microscopic optical potential is successful in reproducing data of NA elastic scattering [4] in the wide range of $40 < E < 250$ MeV from light to heavy targets. Above the pion production threshold, resonance and meson production effects are evident. Recently, a bare NN interaction was extrapolated to reproduce the NN scattering data to 2.5 GeV by adding a complex potential phenomenologically [7], and the g -matrix interaction constructed from the complex NN interaction was also successful in reproducing the NA scattering at $40 < E < 800$ MeV [5].

In many applications, use of a nonlocal NA potential is impractical. For example, in ${}^8\text{B}+\text{A}$ scattering the projectile easily breaks up into ${}^7\text{Be}$ and p. This projectile breakup processes are described by solving the scattering problem of three-body system ${}^7\text{Be}+\text{p}+\text{A}$. If all potentials are local in the system, this problem can be solved by the method of continuum-discretized coupled channels (CDCC) [8, 9]. If the potential between p and A and/or the potential between ${}^7\text{Be}$ and A is nonlocal, this is not easy. For such cases, use of an equivalent local potential is quite practical, if it is accurate. Brieva and Rook (BR) proposed an approximate form of the equivalent local potential [1]. This is commonly used in many applications; for example see Refs. [6, 10] and references therein. However, the validity of

the approximate form is not shown yet.

In this paper, we show the validity of the BR localization over the wide range of $65 < E < 800$ MeV, comparing the scattering solution of the non-local NA potential with that of the BR-type local potential. As a typical case, we consider the $p+^{90}\text{Zr}$ scattering. The BR localization is composed of three approximations. We show that one of the three is redundant, and test the remaining two separately.

In Sec. II, the method of solving the Schrödinger equation with the non-local NA potential and the way of getting the ground-state wave function of target nucleus are presented. In Sec. III, the BR localization is recapitulated. In Sec. IV, the validity of the BR localization and the related topics are argued. Section V is devoted to summary.

II. FORMULATION

In the g -matrix approach [1, 2, 3, 4, 6], the microscopic NA optical potential is constructed by folding the g -matrix interaction g^{ST} with the ground-state density of target nucleus (A), where S (T) is the spin (isospin) of the N+N system. In this procedure, the antisymmetrization between an incident nucleon and target nucleons in A is taken care of by using g^{ST} which is properly antisymmetric with respect to the exchange of the colliding nucleons, since the prescription is shown to be a good approximation [11, 12]. In the approximation, the folding potential is expressed by the sum of a local direct term $U^{\text{DR}}(\mathbf{R})$ and a nonlocal exchange term $U^{\text{EX}}(\mathbf{R}, \mathbf{r})$ [13]. Hence, the elastic scattering can be described by solving the Schrödinger equation

$$\left[-\frac{\hbar^2}{2\mu} \nabla_R^2 + U^{\text{DR}}(\mathbf{R}) + V_c(R) \delta_{-1/2}^{\nu_1} - E \right] \chi_{\mathbf{K}, \nu_1}(\mathbf{R}) = \int U^{\text{EX}}(\mathbf{R}, \mathbf{r}) \chi_{\mathbf{K}, \nu_1}(\mathbf{r}) d\mathbf{r} \quad (1)$$

for the relative wave function $\chi_{\mathbf{K}, \nu_1}(\mathbf{R})$, where \mathbf{R} stands for the coordinate of incident nucleon (N) from the center-of-mass of A, \mathbf{r} is the coordinate of nucleon in A from the center-of-mass of A, $V_c(R)$ is the Coulomb potential, $\hbar\mathbf{K}$ (E) is an incident momentum (energy), and $\nu_1 = 1/2$ for neutron scattering and $-1/2$ for proton one. We assume that the target nucleus is much heavier than N. The relativistic kinematics is taken by defining the reduced mass μ as $\mu = \sqrt{m_N^2 + (p/c)^2}$ with p and m_N the momentum and rest mass of N.

In this paper, we consider only the central part of the microscopic optical potential, since it is a main component of the folding potential. We also assume that the ground state of

A is described by a single determinant of single-nucleon wave functions $\varphi_{\nu_2;nljj_z}(\mathbf{r}, \xi)$, each classified with the z -component ν_2 of isospin, the principal quantum number n , the angular momentum l , and the total angular momentum j and its z -component j_z , where ξ is the internal coordinate of the spin wave function $\eta_{1/2}$ of nucleon. In this case, $U^{\text{DR}}(\mathbf{R})$ and $U^{\text{EX}}(\mathbf{R}, \mathbf{r})$ are given by [1, 2, 3, 4]

$$U^{\text{DR}}(\mathbf{R}) = \sum_{\nu_2, T_z} \int \rho_{\nu_2}(\mathbf{r}) g_{T_z}^{\text{DR}}(s; \rho_{\nu_2}) d\mathbf{r}, \quad (2)$$

$$U^{\text{EX}}(\mathbf{R}, \mathbf{r}) = \sum_{\nu_2, T_z} \rho_{\nu_2}(\mathbf{R}, \mathbf{r}) g_{T_z}^{\text{EX}}(s; \rho_{\nu_2}) \quad (3)$$

with

$$\rho_{\nu_2}(\mathbf{r}) = \sum_{nljj_z} \int \varphi_{\nu_2;nljj_z}^*(\mathbf{r}, \xi) \varphi_{\nu_2;nljj_z}(\mathbf{r}, \xi) d\xi, \quad (4)$$

$$\rho_{\nu_2}(\mathbf{R}, \mathbf{r}) = \sum_{nljj_z} \int \varphi_{\nu_2;nljj_z}^*(\mathbf{r}, \xi) \varphi_{\nu_2;nljj_z}(\mathbf{R}, \xi) d\xi, \quad (5)$$

$$g_{T_z=\pm 1}^{\text{DR}}(s; \rho_{\nu_2}) = \frac{1}{4} \{g^{01}(s; \rho_{\nu_2}) + 3g^{11}(s; \rho_{\nu_2})\} \delta_{T_z}^{\nu_1+\nu_2}, \quad (6)$$

$$g_{T_z=0}^{\text{DR}}(s; \rho_{\nu_2}) = \frac{1}{8} \{g^{01}(s; \rho_{\nu_2}) + 3g^{10}(s; \rho_{\nu_2}) + g^{00}(s; \rho_{\nu_2}) + 3g^{11}(s; \rho_{\nu_2})\} \delta_{T_z}^{\nu_1+\nu_2}, \quad (7)$$

$$g_{T_z=\pm 1}^{\text{EX}}(s; \rho_{\nu_2}) = \frac{1}{4} \{-g^{01}(s; \rho_{\nu_2}) + 3g^{11}(s; \rho_{\nu_2})\} \delta_{T_z}^{\nu_1+\nu_2}, \quad (8)$$

$$g_{T_z=0}^{\text{EX}}(s; \rho_{\nu_2}) = \frac{1}{8} \{-g^{01}(s; \rho_{\nu_2}) - 3g^{10}(s; \rho_{\nu_2}) + g^{00}(s; \rho_{\nu_2}) + 3g^{11}(s; \rho_{\nu_2})\} \delta_{T_z}^{\nu_1+\nu_2}, \quad (9)$$

where $\mathbf{s} = \mathbf{r} - \mathbf{R}$. The g matrix interaction g^{ST} is a function of E and the single-particle density $\rho_{\nu_2}(r_g)$, where $r_g = |\mathbf{r}_g|$ for the location \mathbf{r}_g at which the effective interaction works. As for the g matrix interaction, we take a sophisticated version of the Melbourne interaction [4] that is constructed from the Bonn-B NN potential [14] and includes a modification due to the pion-production effect [7]. Since the interaction has a finite range, r_g can not be determined uniquely. Possible choices are (i) $r_g = r$, (ii) $r_g = R$ and (iii) $r_g = r_m \equiv |\mathbf{r} + \mathbf{R}|/2$. This ambiguity is referred to as the r_g -ambiguity in this paper. The r_g -ambiguity is small, as shown later in Fig. 8. We then take choice (i). We will return to this point below.

Expanding $g_{T_z}^{\text{DR}}$ into a series of multipoles,

$$g_{T_z}^{\text{DR}}(s; \rho) = \sum_{\lambda} 4\pi \frac{(-)^{\lambda}}{\hat{\lambda}} g_{T_z; \lambda}^{\text{DR}}(r, R; \rho) \left[Y_{\lambda}(\hat{\mathbf{R}}) \otimes Y_{\lambda}(\hat{\mathbf{r}}) \right]_{00}, \quad (10)$$

one can get a simple form of

$$U^{\text{DR}}(R) = 4\pi \sum_{\nu_2, T_z} \int \rho_{\nu_2}(r) g_{T_z; 0}^{\text{DR}}(r, R; \rho_{\nu_2}) r^2 dr. \quad (11)$$

In this form, $U^{\text{DR}}(R)$ is a function of $R = |\mathbf{R}|$.

The scattering wave function $\chi_{\mathbf{K},\nu_1}(\mathbf{r})$ is expanded into partial waves $\chi_{K\nu_1,L'}(r)$:

$$\chi_{\mathbf{K},\nu_1}(\mathbf{r}) = \frac{4\pi}{Kr} \sum_{L'M'} \chi_{K\nu_1,L'}(r) i^{L'} Y_{L'M'}^* \left(\hat{\mathbf{K}} \right) Y_{L'M'}(\hat{\mathbf{r}}). \quad (12)$$

Inserting Eq. (12) into Eq. (1), multiplying the equation by $Y_{LM}^*(\hat{\mathbf{R}})$ from the left and integrating it over the solid angle $\hat{\mathbf{R}}$, one can get an equation for $\chi_{K\nu_1,L}$ as

$$\begin{aligned} & \left[-\frac{\hbar^2}{2\mu} \frac{d^2}{dR^2} + \frac{\hbar^2}{2\mu} \frac{L(L+1)}{R^2} + U^{\text{DR}}(R) + V_c(R) \delta_{-1/2}^{\nu_1} - E \right] \chi_{K\nu_1,L}(R) \\ &= \sum_{\nu_2, T_z; nlj\lambda} \frac{\hat{j}^2}{\hat{j}^2} (L0\lambda 0|l0)^2 \int \phi_{\nu_2;nlj}^*(r) g_{T_z;\lambda}^{\text{EX}}(r, R; \rho_{\nu_2}(r_g)) \phi_{\nu_2;nlj}(R) \chi_{K\nu_1,L}(r) dr, \quad (13) \end{aligned}$$

where $g_{T_z}^{\text{EX}}$ has been expanded into multipoles $g_{T_z;\lambda}^{\text{EX}}$ just as in Eq. (10), and $\phi_{\nu;nlj}(r)$ is the radial part of the single-nucleon wave function $\varphi_{\nu;nljj_z}(\mathbf{r}, \xi)$. In the derivation of Eq. (13), $\delta_{L'L}$ came out in L' summation, so that $\chi_{K\nu_1,L}(R)$ on the left hand side has the same angular momentum L as $\chi_{K\nu_1,L}(r)$ on the right hand side. This is a consequence of the fact that Eq. (1) is rotational invariant in the coordinate space. In the present paper, $\chi_{K\nu_1,L}(R)$ is obtained by solving Eq. (13) iteratively. In Eq. (13), each multipole $g_{T_z;\lambda}^{\text{EX}}$ depends on r_g through ρ_{ν_2} , but it includes no information on an angle between vectors \mathbf{r} and \mathbf{R} . Hence, we can not take choice (iii), which is commonly used in the BR localization, in the form of Eq. (13). For this reason in addition to the reason that the r_g -ambiguity itself is small, we take choice (i) in the present study.

As for the ground state wave function of target nucleus, it is desirable to be as realistic as possible, and to be calculated theoretically because we are planning to apply the formulation to unstable nuclei where no experimental data are expected. Therefore, we employ the Hartree-Fock (HF) calculation with the finite-range Gogny force[15] as an effective interaction. In particular, the D1S parameter-set[16] is adopted, which is applied widely and successfully to many nuclear structure problems (see, e.g., Ref.[17]). The standard method to solve the HF equation with the Gogny force is to expand the single-nucleon wave functions in terms of the harmonic oscillator basis. It is, however, not very accurate when the wave functions extend far outside nucleus due to the weak-binding, which is characteristic in unstable nuclei. The Gaussian expansion method (GEM) [18, 19] is a powerful method to treat such a problem of the spacially extended wave functions, and it has been applied for solving the HF[20] and HFB (Hartree-Fock-Bogoliubov)[21] equations. We have developed

our own program to solve the HF and HFB equations by the Gaussian expansion, where the merit of the Gaussian form of the interaction is fully utilized.

In the present work, the target nucleus is ^{90}Zr , which is a stable nucleus and the method of the harmonic oscillator basis expansion works. However, the use of the Gaussian basis expansion is still preferable because the calculation of the matrix elements of the g -matrix in Eq. (13) can be done easily and accurately. We have calculated the ground state of ^{90}Zr by the HFB method. It is found that the neutron pairing gap vanishes because of the $N = 50$ shell closure and the proton pairing gap is also very small due to the subshell $Z = 40$. The energy gain by the pairing correlation is less than 100 keV, and its effect on the density $\rho_\nu(r)$ is less than 1.5%. Therefore, we use the HF wave function neglecting the pairing correlation in this work. In more detail, the radial part of the single-nucleon wave functions in each $(\nu; lj)$ -channel are expanded by the Gaussian functions,

$$\phi_{\nu;nlj}(r) = \sum_{i=1}^{n_g} C_{n,i}^{(\nu;lj)} e^{-(r/\lambda_i)^2}, \quad (14)$$

where we take $n_g = 14$ and their ranges λ_i ($i = 1, \dots, n_g$) are chosen to be from 1 to 5 fm by geometric progression according to GEM[18, 19]; they are an almost optimal choice in the case of $n_g = 14$. The coefficients $C_{n,i}^{(\nu;lj)}$ are determined by the HF variational equation. The resultant binding energy of ^{90}Zr is 785.995 MeV, which is compared to the experimental value 783.894 MeV. This result corresponds to the calculation employing 25 shells ($N_{\text{osc}} \leq 24$) in the harmonic oscillator basis. We believe that the obtained wave function is realistic enough to perform the test of the localization of optical potential.

III. THE BRIEVA-ROOK LOCALIZATION

A local potential $U_{\text{loc}}^{\text{EX}}(\mathbf{R})$ trivially equivalent to the nonlocal potential $U^{\text{EX}}(\mathbf{R}, \mathbf{r})$ is defined by

$$U_{\text{loc}}^{\text{EX}}(\mathbf{R})\chi_{\mathbf{K},\nu_1}(\mathbf{R}) = \int U^{\text{EX}}(\mathbf{R}, \mathbf{r})\chi_{\mathbf{K},\nu_1}(\mathbf{r}) d\mathbf{r}. \quad (15)$$

Brieva and Rook derived an approximate form $U_{\text{BR}}^{\text{EX}}(\mathbf{R})$ to the equivalent local potential $U_{\text{loc}}^{\text{EX}}(\mathbf{R})$ [1]. The derivation is composed of three approximations. The first approximation, called the local semi-classical approximation (LSCA) [22], is

$$\chi_{\mathbf{K},\nu_1}(\mathbf{r}) = \chi_{\mathbf{K},\nu_1}(\mathbf{R} + \mathbf{s}) \approx \chi_{\mathbf{K},\nu_1}^{\text{LSC}}(\mathbf{r}) \equiv \chi_{\mathbf{K},\nu_1}(\mathbf{R}) e^{i\mathbf{K}(\mathbf{R})\cdot\mathbf{s}}, \quad (16)$$

where the local momentum $\hbar\mathbf{K}(\mathbf{R})$ is parallel to the flux of the scattering wave at \mathbf{R} and its magnitude is determined to satisfy

$$\hbar K(\mathbf{R}) = [2\mu(E - V_c(R)\delta_{-1/2}^{\nu_1} - U^{\text{DR}}(\mathbf{R}) - U_{\text{loc}}^{\text{EX}}(\mathbf{R}))]^{1/2}, \quad (17)$$

i.e., $\hbar\mathbf{K}(\mathbf{R})$ is evaluated self-consistently. LSCA has been successfully applied to studies on cross sections and spin observables for multistep direct ($p, p'x$) and (p, nx) processes as well as hyperon production cross sections [23].

LSCA yields a local form of

$$U_{\text{LSC}}^{\text{EX}}(\mathbf{R}) = \sum_{\nu_2, T_z} \int \rho_{\nu_2}(\mathbf{R}, \mathbf{r}) g_{T_z}^{\text{EX}}(s; \rho_{\nu_2}(r_g)) e^{i\mathbf{K}(\mathbf{R}) \cdot \mathbf{s}} ds. \quad (18)$$

The local potential $U_{\text{LSC}}^{\text{EX}}(\mathbf{R})$ of Eq. (18) is a function of the radial component R and the angle θ between vectors \mathbf{R} and $\mathbf{K}(\mathbf{R})$, as shown later. Obviously, LSCA is getting better as E increases. Actually, LSCA is good for $E \gtrsim 65$ MeV, as shown later in Sec. IV.

The second approximation, called the local Fermi-gas approximation (LFGA) [24], is an approximation to the single-particle mixed density $\rho_{\nu_2}(\mathbf{R}, \mathbf{r})$:

$$\rho_{\nu_2}(\mathbf{R}, \mathbf{r}) \approx \rho_{\nu_2}(r_m) \frac{3}{(sk_{\nu_2}^{\text{F}}(r_g))^3} [\sin(sk_{\nu_2}^{\text{F}}(r_g)) - sk_{\nu_2}^{\text{F}}(r_g) \cos(sk_{\nu_2}^{\text{F}}(r_g))] \equiv \rho_{\nu_2}^{\text{LFG}}(\mathbf{R}, \mathbf{r}), \quad (19)$$

where $k_{\nu_2}^{\text{F}}(r_g)$ is related to $\rho_{\nu_2}(r_g)$ as

$$\rho_{\nu_2} = \frac{(k_{\nu_2}^{\text{F}})^3}{3\pi^2}. \quad (20)$$

LFGA is known to be a good approximation for small values of s [24]. The third approximation is expressed by

$$e^{i\mathbf{K}(\mathbf{R}) \cdot \mathbf{s}} \approx j_0(K(\mathbf{R})s), \quad (21)$$

where j_X is the spherical Bessel function. This approximation is good when $j_0(K(\mathbf{R})s) \ll j_X(K(\mathbf{R})s)$ for $X \geq 1$. This condition is well satisfied when $K(\mathbf{R})s \lesssim 1$. In Eq. (18), the range of the integrand is about 0.5 fm because of the presence of the short-ranged interaction $g_{T_z}^{\text{EX}}$. In the surface region of A that is important for forward NA scattering, $K(\mathbf{R})$ approximately equals the asymptotic wave number K . Hence, Eq. (21) is good at least for $K \lesssim 2 \text{ fm}^{-1}$ ($E \lesssim 80$ MeV). Eventually, the BR-type equivalent local potential $U_{\text{BR}}^{\text{EX}}(\mathbf{R})$ is obtained by

$$U_{\text{BR}}^{\text{EX}}(R) = \sum_{\nu_2, T_z} \int \rho_{\nu_2}^{\text{LFG}}(\mathbf{R}, \mathbf{r}) g_{T_z}^{\text{EX}}(s; \rho_{\nu_2}(r_g)) j_0(K(R)s) ds. \quad (22)$$

In the above derivation, LSCA is good for $E \gtrsim 65$ MeV, while Eq. (21) is applicable for $E \lesssim 80$ MeV. However, as shown in Sec. IV A, the BR-type local potential $U_{\text{BR}}(R) \equiv U^{\text{DR}}(R) + U_{\text{BR}}^{\text{EX}}(R)$ gives almost the same elastic-scattering cross section as that obtained by the exact calculation for $65 \leq E \leq 800$ MeV. This means that the above derivation is not sufficient. Actually, as shown in Sec. IV B, Eq. (22) is derivable from Eq. (18) without the approximation (21), that is, the approximation is redundant. Although, in the original work [1] of Brieva and Rook, the local momentum $\hbar\mathbf{K}(\mathbf{R})$ is assumed to be parallel to the asymptotic momentum $\hbar\mathbf{K}$, it is not necessary because Eq. (22) does not depend on the direction of $\mathbf{K}(\mathbf{R})$. Since LSCA itself is more accurate for $\hbar\mathbf{K}(\mathbf{R})$ parallel to the flux of the scattering wave at \mathbf{R} , we should think that the direction is also taken in the BR localization.

IV. RESULTS

A. Proton elastic-scattering from ^{90}Zr

Figure 1 presents the differential cross sections of the proton elastic scattering from ^{90}Zr at (a) $E = 65$ MeV, (b) 185 MeV, (c) 400 MeV and (d) 800 MeV. For each panel, the horizontal lower (upper) scale represents the transferred wave number q (the scattering angle θ_{cm}). The solid curves represent results of the exact calculation in which Eq. (1) is solved numerically. In the dashed curves, the medium effect is switched off from the exact calculation by taking $g^{ST}(s; \rho_{\nu_2} = 0)$ in Eqs. (2) and (3). In the dotted curves, the exchange effect is neglected from the exact calculation by setting $g_{T_2;\lambda}^{\text{EX}} = 0$ in Eq. (1). Thus, the exchange effect is large at least up to $E = 800$ MeV, and the medium effect is significant up to $E = 400$ MeV.

Now, the validity of the BR localization is tested. Figure 2 presents the same quantities as in Fig. 1, but with different calculations. The solid curves represent results of the exact calculation of Eq. (1), while the dashed curves do results of the BR-type local potential $U_{\text{BR}}(R)$, that is, the Schrödinger equation with $U_{\text{BR}}(R) \equiv U^{\text{DR}}(R) + U_{\text{BR}}^{\text{EX}}(R)$ is solved numerically. Seeing the difference between the two types of lines around $q = 3.5 \text{ fm}^{-1}$, one can find that the error of the BR localization is getting small as E increases. For $E = 65$ MeV, the error is small at $q \lesssim 1.7 \text{ fm}^{-1}$ where the data are available, although it is sizable at large q around 3.5 fm^{-1} . Thus, the BR localization is good for $65 \text{ MeV} \leq E \leq 800 \text{ MeV}$. We discuss this point in Sec. IV B in detail.

In Fig. 3, the exact wave function (solid curve) of the Schrödinger equation Eq. (1) is compared with the approximate wave function calculated with $U_{\text{BR}}(R)$ for the case of the $p+^{90}\text{Zr}$ scattering at $L = 8$, where the elastic partial cross section $\sigma_L^{\text{el}} = \pi(2L+1)|1-S_L|^2/K^2$ calculated with the elastic S -matrix element S_L becomes maximum. For both $E = 65$ MeV and 185 MeV, the approximation wave functions are very close to the exact ones.

B. Validity of the BR localization

First, we show the numerical test of LSCA, together with a simplified version of LSCA in which the absolute value of the local momentum, $\hbar K(\mathbf{R})$, is replaced by that of the asymptotic momentum $\hbar K$. This version is referred to as LSCA-A in this paper. LSCA-A is, if justified, very useful since LSCA-A makes it much simpler the numerical task to obtain $U_{\text{BR}}^{\text{EX}}(R)$.

For this purpose, we consider the potential scattering and take $U_{\text{BR}}(R) = U^{\text{DR}}(R) + U_{\text{BR}}^{\text{EX}}(R)$ as the potential. The exact wave function $\chi_{\mathbf{K},\nu_1}(\mathbf{r})$ of the potential scattering is compared with the approximate wave functions $\chi_{\mathbf{K},\nu_1}^{\text{LSA}}(\mathbf{r})$ and $\chi_{\mathbf{K},\nu_1}^{\text{LSC-A}}(\mathbf{r})$ based on LSCA and LSCA-A, respectively. The wave functions are invariant under the rotation around the z axis, and hence the azimuthal angle φ of vector \mathbf{R} can be set to zero. As an example, vector \mathbf{R} is fixed to $(R, \theta, \varphi) = (5 \text{ fm}, \pi/3, 0)$, and vector \mathbf{s} in Eq. (16) is varied in a direction either parallel or perpendicular to \mathbf{R} . For convenience, a variation of vector \mathbf{s} in the direction parallel (perpendicular) to \mathbf{R} is denoted by s_r (s_θ); precisely, $\mathbf{s}_r = (\mathbf{s} \cdot \mathbf{n})\mathbf{n}$ with $\mathbf{n} = \mathbf{R}/R$ and $\mathbf{s}_\theta = \mathbf{s} - s_r\mathbf{n}$. Note that LSCA is expected to work well if the potential around \mathbf{R} varies slowly within the wave length of $\chi_{\mathbf{K},\nu_1}(\mathbf{r})$. Thus, the choice of $R = 5$ fm can severely test the validity of LSCA.

Figure 4 represents the exact and approximate wave functions of the $p+^{90}\text{Zr}$ elastic scattering at $E = 400$ MeV. In panels (a) and (b) where s_θ is varied with s_r fixed to 0, the wave functions $\chi_{\mathbf{K},\nu_1}^{\text{LSC}}(\mathbf{r})$ (dashed curves) and $\chi_{\mathbf{K},\nu_1}^{\text{LSC-A}}(\mathbf{r})$ (dotted curves) agree with $\chi_{\mathbf{K},\nu_1}(\mathbf{r})$ (solid curves) within the range of the g -matrix interaction, i.e. at $s \lesssim 1.5$ fm. This is the case also for panels (c) and (d) where s_r is varied with s_θ fixed to 0. Further, $\chi_{\mathbf{K},\nu_1}^{\text{LSC}}(\mathbf{r})$ is identical to $\chi_{\mathbf{K},\nu_1}^{\text{LSC-A}}(\mathbf{r})$ at $s \lesssim 1.5$ fm. Thus, LSCA and LSCA-A are accurate for high E . At slightly lower energy of 185 MeV, as shown in Fig. 5, the accuracy of LSCA and LSCA-A is almost the same as at 400 MeV. Figure 6 shows the results at 65 MeV.

One sees that LSCA and LSCA-A still work well, although its accuracy becomes slightly worse than for $E \geq 185$ MeV. Thus, we conclude that LSCA and LSCA-A are applicable for $E \gtrsim 65$ MeV. Actually, as shown in Fig. 7, the elastic-scattering cross section for p+⁹⁰Zr at 65 and 185 MeV calculated with LSCA-A in the BR localization agrees well with the result of the standard BR calculation with LSCA; particularly at 185 MeV, the difference between the two is within the thickness of lines.

Next, we consider the remaining two approximations, i.e., LFGA and Eq. (21). One can find, however, the latter is redundant, if an extended LFGA below is justified. We consider the following approximation for the mixed density:

$$\rho_{\nu_2}(\mathbf{R}, \mathbf{r}) \approx \rho_{\nu_2}(R) \frac{3}{(sk_{\nu_2}^F(R))^3} [\sin(sk_{\nu_2}^F(R)) - sk_{\nu_2}^F(R) \cos(sk_{\nu_2}^F(R))] \equiv \rho_{\nu_2}^{\text{LFG-R}}(\mathbf{R}, \mathbf{r}). \quad (23)$$

This approximation is referred to as LFGA- R . Note that $\rho_{\nu_2}^{\text{LFG-R}}(\mathbf{R}, \mathbf{r})$ is nothing but $\rho_{\nu_2}^{\text{LFG}}(\mathbf{R}, \mathbf{r})$ of Eq. (19), with r_m and r_g replaced by R . Obviously, as long as LFGA is valid, LFGA- R is also good for R larger than the range of the NN interaction $s \approx 0.5$ fm. Inserting Eq. (23) into Eq. (18) leads to Eq. (22) without Eq. (21), since $\rho_{\nu_2}(\mathbf{R}, \mathbf{r})$ is a function of R and s in LFGA- R . Thus, Eq. (21) is not necessary, when LFGA- R is taken.

The validity of LFGA- R is evaluated by comparing the results of the elastic-scattering cross sections calculated with LFGA and LFGA- R . It is found that in the energy region of $65 \text{ MeV} \leq E \leq 800 \text{ MeV}$, the two calculations show a perfect agreement. Thus, we conclude that Eq. (21), which has imposed an upper limit of E where the BR localization is accurate, is actually redundant because of the good accuracy of LFGA- R . This comes from the fact that, as mentioned above, LFGA itself is a very good approximation to the mixed density. In fact, it turns out that the p+⁹⁰Zr elastic-scattering cross section calculated with LFGA agrees very well with that obtained with explicitly using the mixed density. Another point to be mentioned here is that the simplest formula, Eq. (20), is used for evaluating $k_{\nu_2}^F$ from the one-body density. Our finding clearly shows that Eq. (20) is enough to study the elastic-scattering cross sections; the higher-order corrections to $k_{\nu_2}^F$ [24, 29] are not necessary for this purpose.

Finally, we comment on the r_g -ambiguity of the BR-type local potential. Figure 8 shows the elastic-scattering cross section from ⁹⁰Zr at (a) $E = 65$ MeV, (b) 185 MeV, (c) $E = 400$ MeV and (d) 800 MeV. The solid lines represent results of the BR local potential calculated with choice (i), and the dashed and dotted lines correspond to results of choices

(ii) and (iii), respectively. The differences among the three cases are appreciable only at dips for $E = 65$ MeV. For $E = 185$ MeV, they are appreciable even for tops. For higher E such as $E \gtrsim 400$ MeV, the differences become negligible, since so is the medium effect itself. Thus, the folding potential has an appreciable r_g -ambiguity only around $E = 200$ MeV in which the imaginary part of $U_{\text{BR}}(R)$ is rather weak compared with the case of other E .

V. SUMMARY

We test the BR localization of the microscopic nucleon-nucleus optical potential over the wide range of $65 < E < 800$ MeV and conclude that the localization is valid there. The BR localization is composed of the local semi-classical approximation (LSCA), the local Fermi-gas approximation (LFGA) and Eq. (21), but these approximations can be reduced to two, LSCA and LFGA- R (a modified version of LFGA). The former is reliable at $E \gtrsim 65$ MeV, while the latter is good for any E . The approximate wave functions calculated with the BR-type local potential are very close to the exact ones. Thus, the BR-type local potential is quite useful in many applications, for example, as potentials between A and constituents of weakly bound or unstable projectiles.

Acknowledgements

The authors thank Kawai, Sakuragi and Nakada for their interest to the present subject.

-
- [1] Brieva F A and Rook J R 1977 *Nucl. phys. A* **291** 299
 Brieva F A and Rook J R 1977 *Nucl. phys. A* **291** 317
 Brieva F A and Rook J R 1978 *Nucl. phys. A* **297** 206
- [2] Yamaguchi N, Nagata S and Matsuda T 1983 *Prog. Theor. Phys.* **70** 459
 Yamaguchi N, Nagata S and Michiyama J 1986 *Prog. Theor. Phys.* **76** 1289
- [3] Rikus L, Nakano K and von Geramb H V 1984 *Nucl. Phys. A* **414** 413
 Rikus L and von Geramb H V 1984 *Nucl. Phys. A* **426** 496
- [4] Amos K, Dortmans P J, von Geramb H V, Karataglidis S and Raynal J 2000 *Adv. Nucl. Phys.* **25** 275

- [5] Deb P K and Amos K 2000 *Phys. Rev. C* **62** 024605
- [6] Furumoto T, Sakuragi Y and Yamamoto Y 2008 *Phys. Rev. C* **78** 044610
- [7] von Geramb H V, Amos K A, Labes H and Sander M 1998 *Phys. Rev. C* **58** 1948
- [8] Kamimura M, Yahiro M, Iseri Y, Sakuragi Y, Kameyama H and Kawai M 1986 *Prog. Theor. Phys. Suppl.* **89** 1
Austern N, Iseri Y, Kamimura M, Kawai M, Rawitscher G and Yahiro M 1987 *Phys. Rep.* **154** 125
- [9] Ogata K, Hashimoto S, Iseri Y, Kamimura M and Yahiro M 2006 *Phys. Rev. C* **73** 024605
[arXiv:nucl-th/0505007] and references therein.
- [10] Furumoto T, Sakuragi Y and Yamamoto Y 2009 *Phys. Rev. C* **79** 011601
- [11] Takeda G and Watson K M 1955 *Phys. Rev.* **97** 1336
- [12] Picklesimer A and Thaler R M 1981 *Phys. Rev. C* **23** 42
- [13] Owen L W and Satchler G R 1970 *Phys. Rev. Lett.* **25** 1720
- [14] Machleidt R, Holinde K and Elster Ch 1987 *Phys. Rep.* **149** 1
- [15] Decharge J and Gogny D 1980 *Phys. Rev. C* **21** 1568
- [16] Berger J F, Girod M and Gogny D 1991 *Comp. Phys. Comm.* **63** 365
- [17] Hilaire S and Girod M 2007 *Eur. Phys. J. A* **33** 237 and referenses therein.
- [18] Kamimura M 1988 *Phys. Rev. A* **38** 621
- [19] Hiyama E, Kino Y and Kamimura M 2003 *Prog. Part. Nucl. Phys.* **51** 223
- [20] Nakada H and Sato M 2002 *Nucl. Phys. A* **699** 511
- [21] Nakada H 2006 *Nucl. Phys. A* **764** 117
- [22] Luo Y L and Kawai M 1991 *Phys. Rev. C* **43** 2367
- [23] Ogata K, Hillhouse G C and van der Ventel B I S 2007 *Phys. Rev. C* **76** 021602(R)
Hashimoto S, Kohno M, Ogata K and Kawai M 2008 *Prog. Theor. Phys.* **119** 1005
Ogata K, Watanabe Y, Sun Weili, Kohno M and Kawai M 2002 *Nucl. Phys. A* **703** 152
- [24] Negele J W and Vautherin D 1972 *Phys. Rev. C* **5** 1472
- [25] Sakaguchi H *et al* 1982 *Phys. Rev. C* **26** 944
- [26] Hadberg E *et al* 1971 *Phys. Scr.* **3** 245
- [27] Lee L *et al* 1989 *J. Phys. G: Nucl. Part. Phys.* **15** 91
- [28] Baker F Todd *et al* 1983 *Nucl. Phys. A* **393** 283
- [29] Campi X and Bouyssy A 1978 *Phys. Lett. B* **73** 263

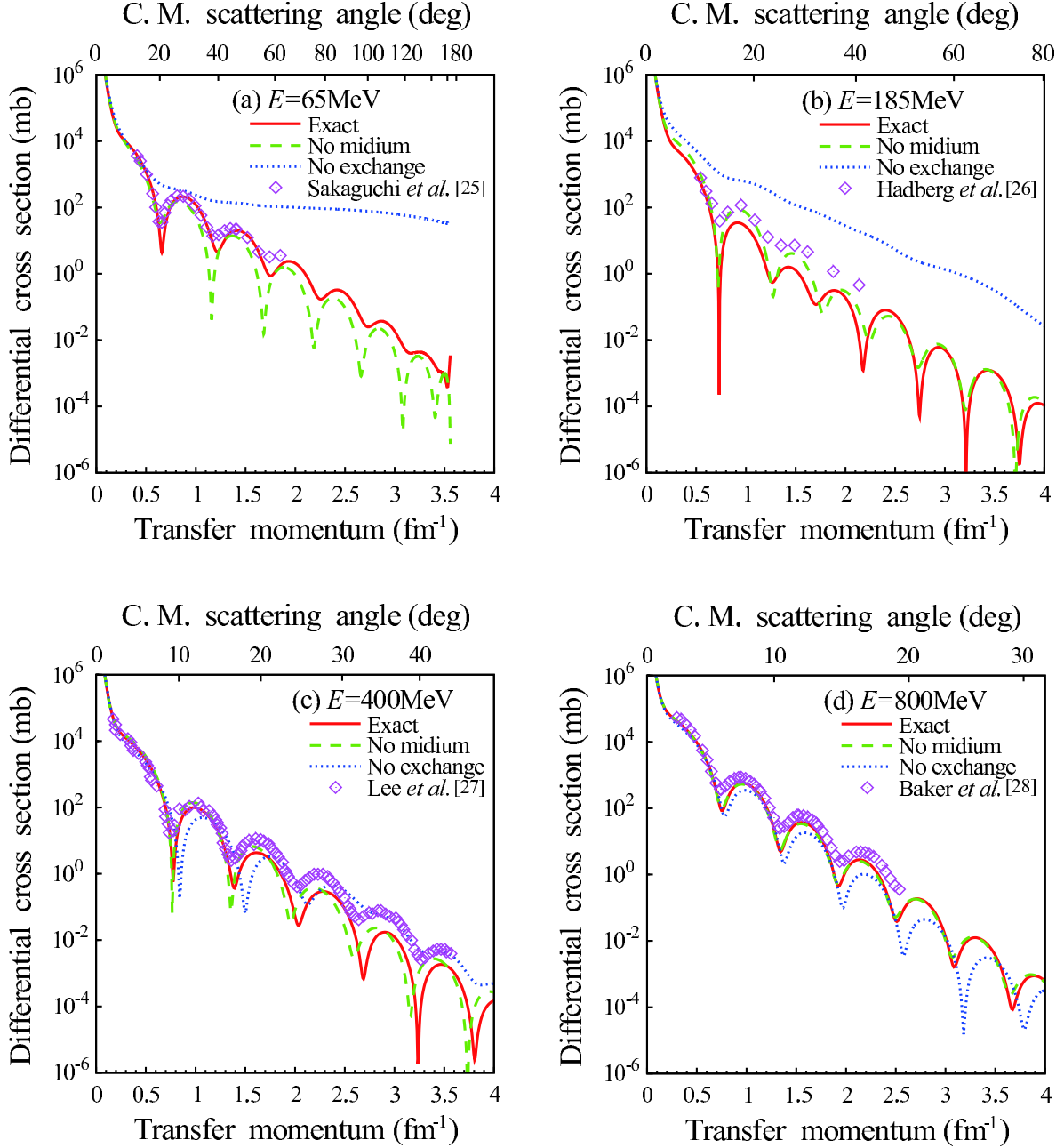


FIG. 1: (color online) The differential cross sections of the proton scattering from ^{90}Zr at (a) $E = 65$ MeV, (b) 185 MeV, (c) 400 MeV and (d) 800 MeV. The solid curves represent the results of the exact calculation, while the dashed (dotted) curves corresponding to the calculation without the medium (exchange) effect. The horizontal lower (upper) scale shows the transferred wave number q (the scattering angle θ_{cm}). Experimental data are taken from Refs. [25, 26, 27, 28].

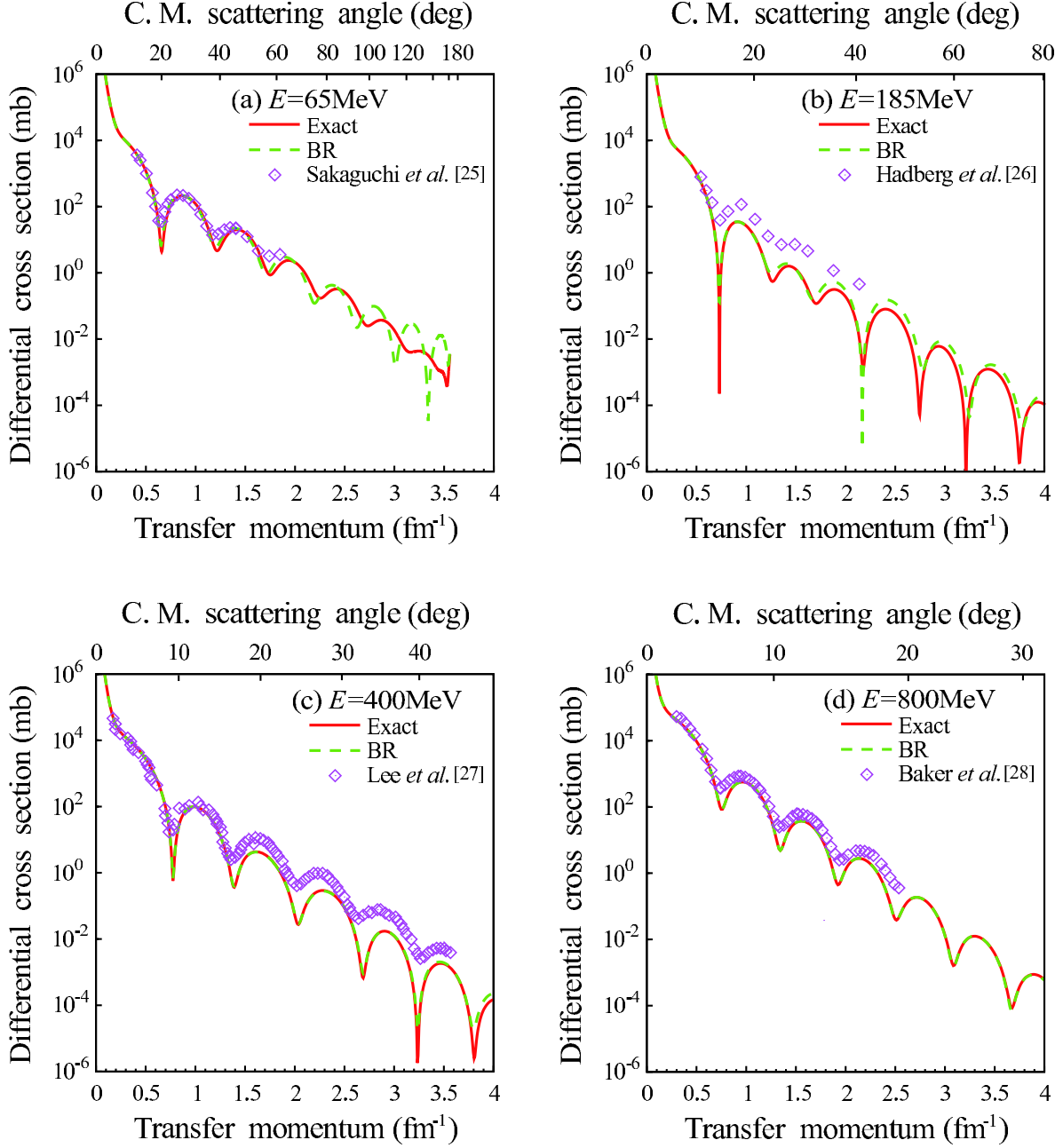


FIG. 2: (color online) Same as in Fig. 1 except that the dashed lines show the results of the BR folding model, i.e., with $U_{\text{BR}}(R)$.

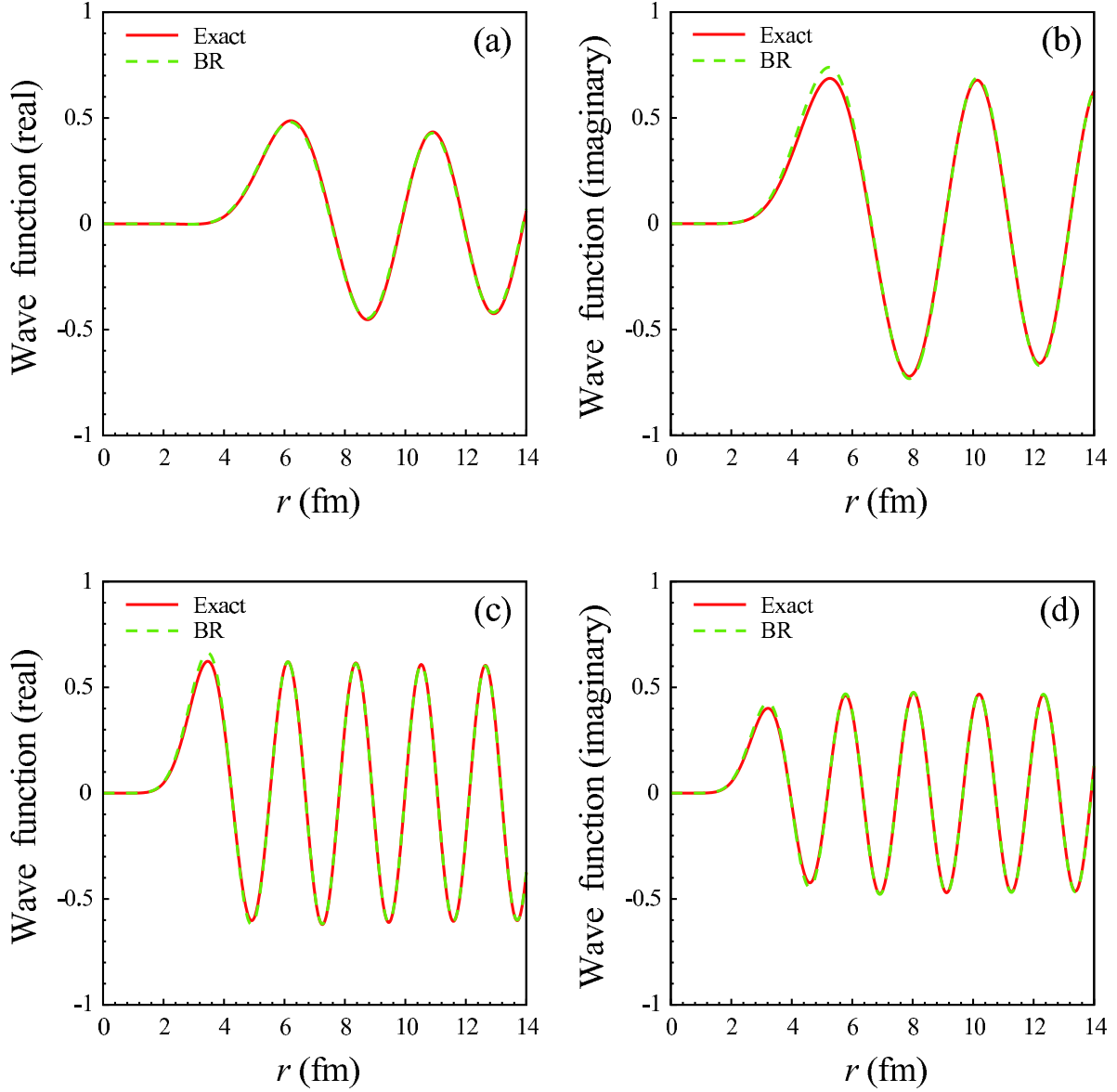


FIG. 3: (color online) The exact and approximate wave functions for the $p+^{90}\text{Zr}$ scattering in the case of $L = 8$. The left and right panels represent the real and imaginary parts of the wave functions, respectively. The upper (lower) panels correspond to $E = 65$ MeV (185 MeV).

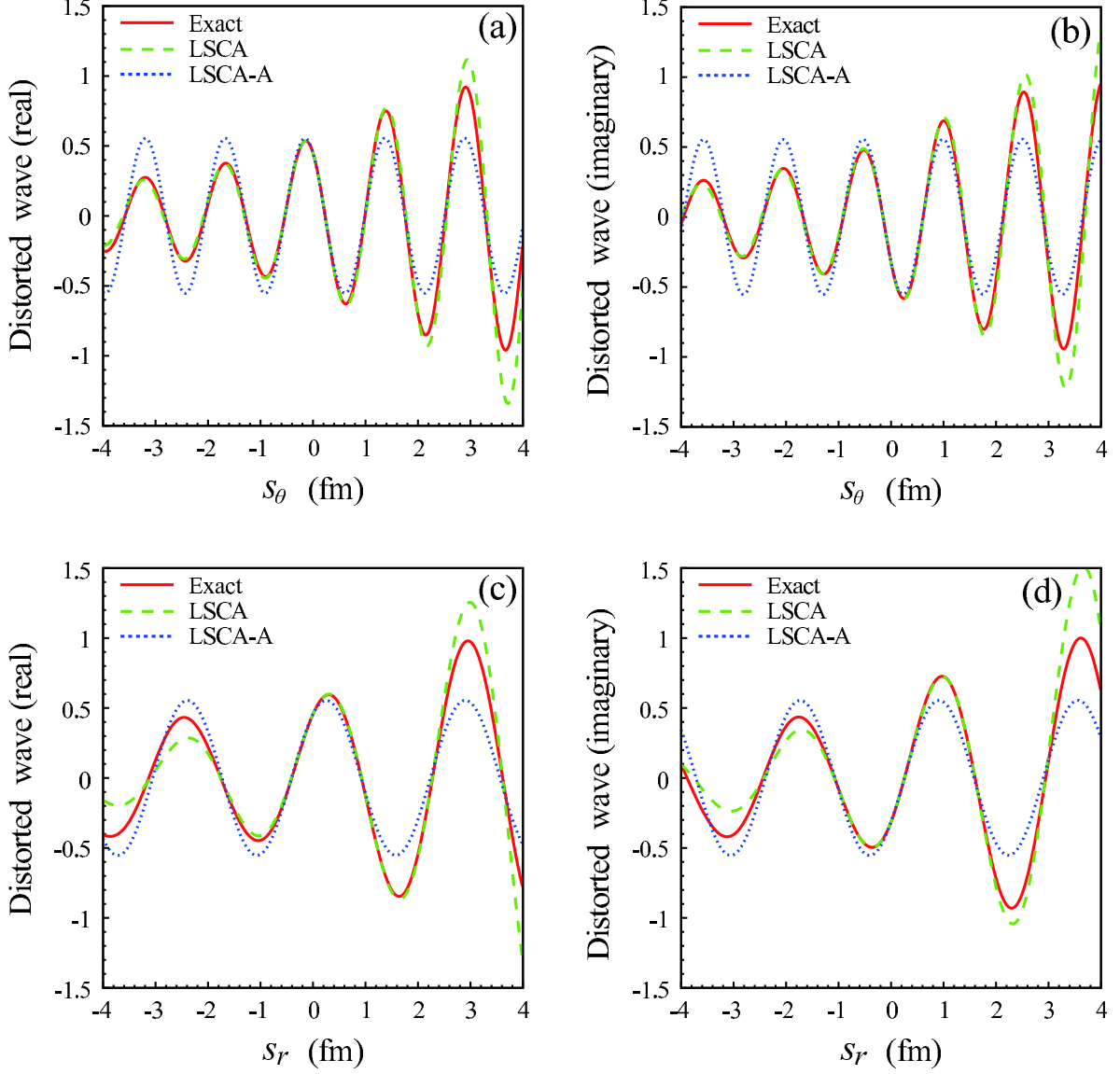


FIG. 4: The exact and approximate wave functions of the $p+^{90}\text{Zr}$ elastic scattering at $E = 400$ MeV. Vector \mathbf{R} is fixed at $\mathbf{R} = (R, \theta) = (5 \text{ fm}, \pi/3)$. In panels (a) and (b) s_θ is varied, while in panels (c) and (d) s_r is varied. The left (right) panels represent the real (imaginary) parts of the wave functions. In LSCA, the direction of vector $\mathbf{K}(\mathbf{R})$ is assumed to be parallel to the flux of the scattering wave at \mathbf{R} . The same assumption is made also for the direction of \mathbf{K} in LSCA-A.

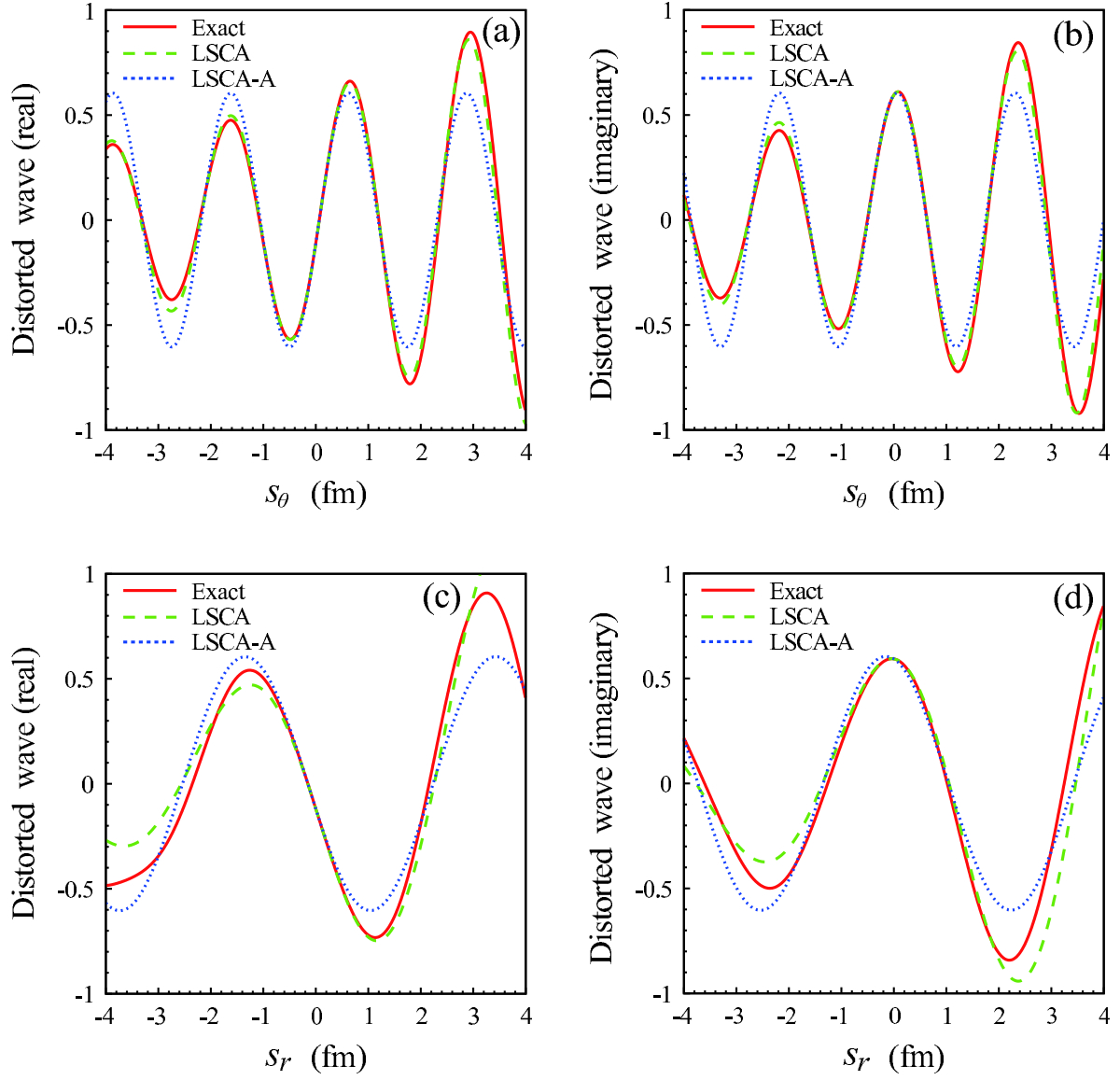


FIG. 5: Same as in Fig. 4 but at $E = 185$ MeV.

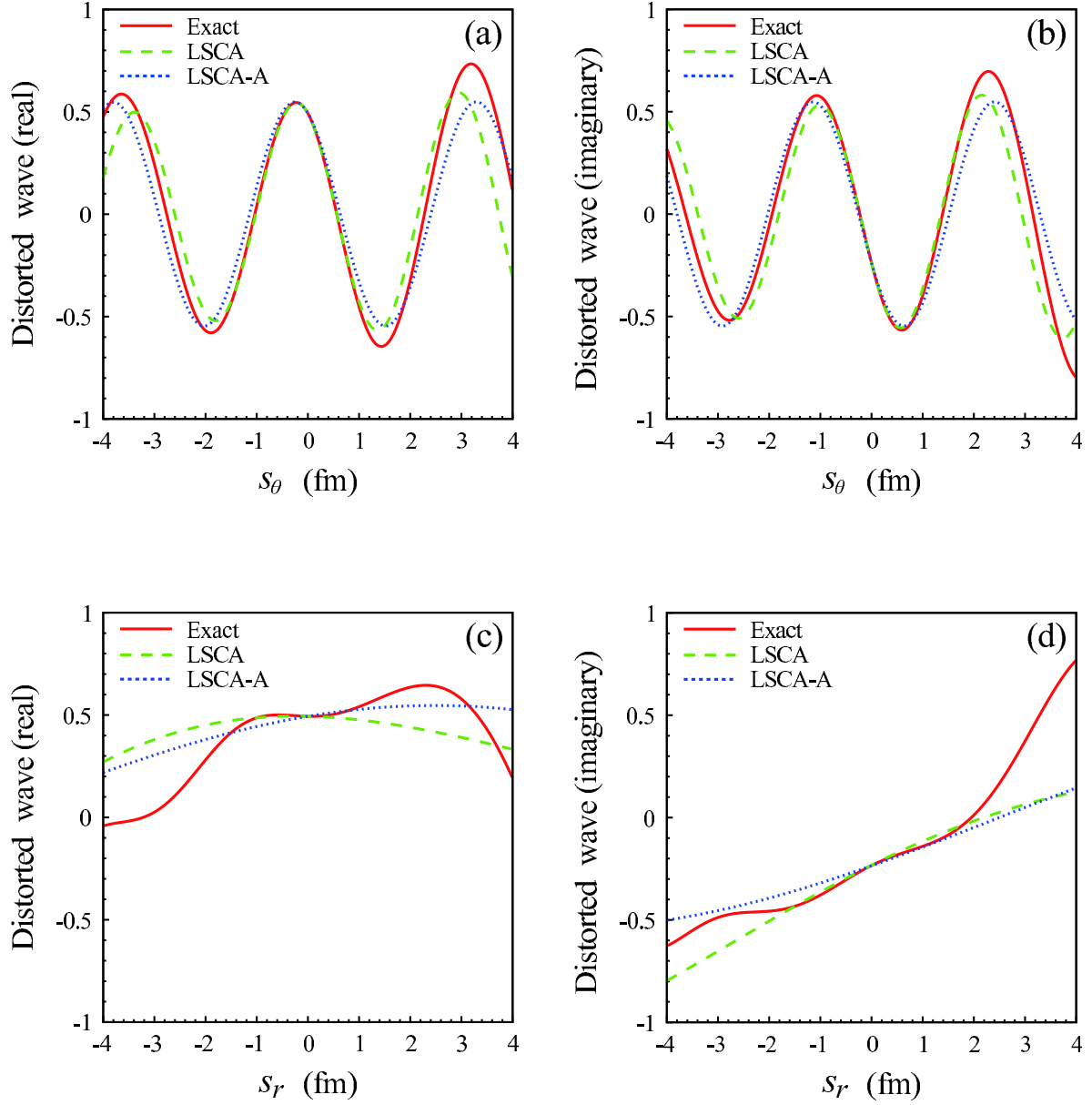


FIG. 6: Same as in Fig. 4 but at $E = 65$ MeV.

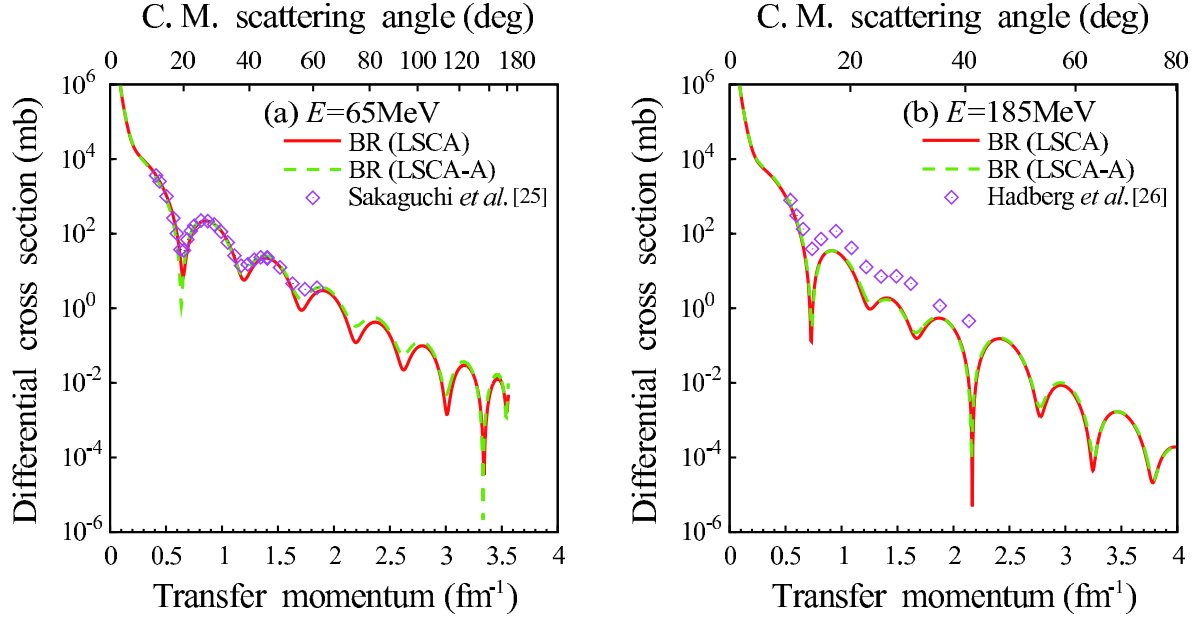


FIG. 7: (color online) The validity of LSCA-A. Panels (a) and (b) represent the differential cross sections of the proton scattering from ^{90}Zr at $E = 65$ MeV and 185 MeV, respectively. The dashed curves denote the results of the BR local potential in which LSCA-A is taken instead of LSCA, while the solid curves show the results of the ordinary BR local potential.

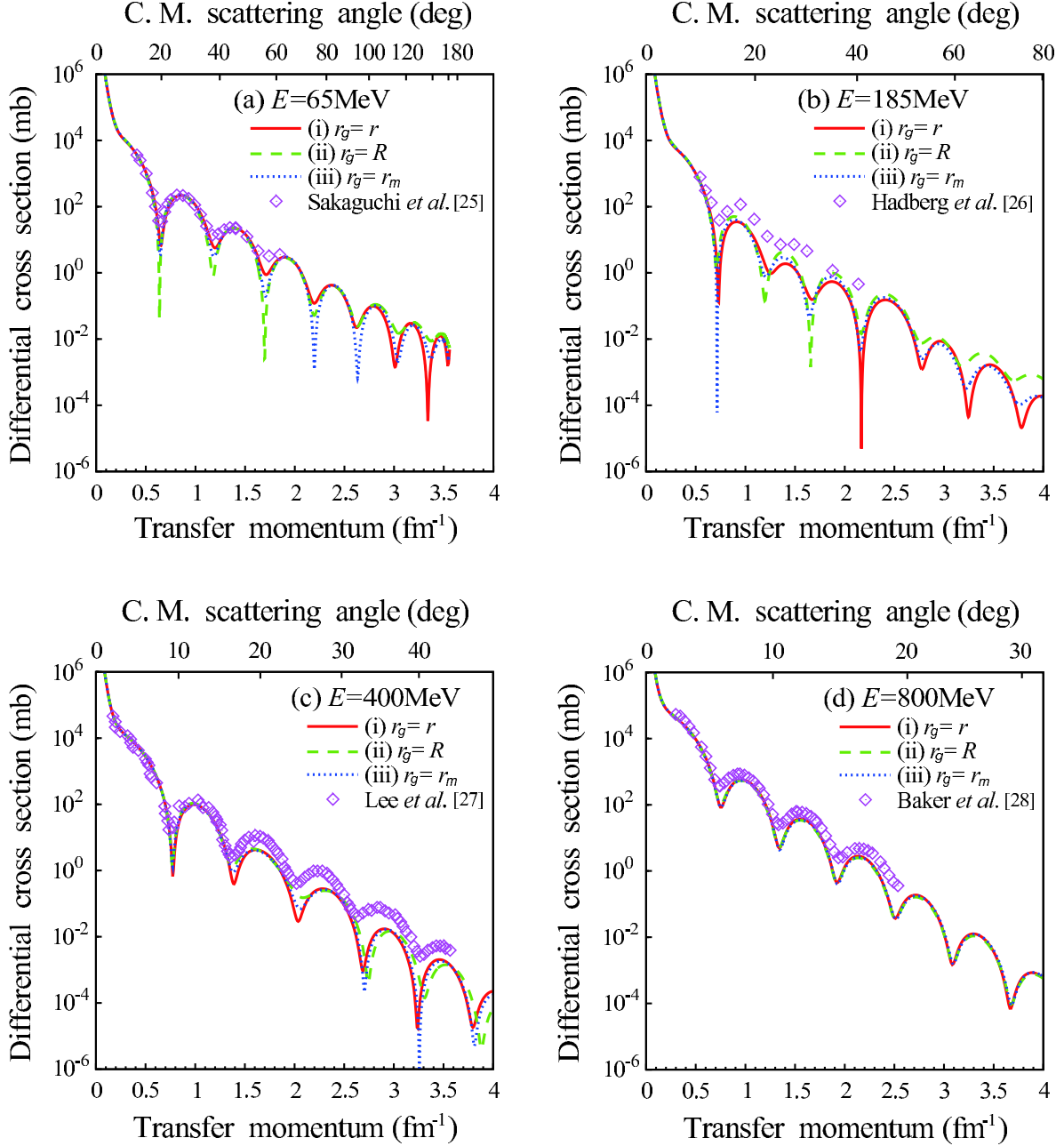


FIG. 8: (color online) The r_g -ambiguity of the BR local potential for the elastic-scattering cross section from ^{90}Zr at (a) $E = 65$ MeV, (b) 185 MeV, (c) $E = 400$ MeV and (d) 800 MeV. The solid, dashed and dotted curves stand for the results of the BR local potential calculated with choices (i), (ii) and (iii) for r_g , respectively. See the text for details.